IEEE Photonics Journal
An IEEE Photonics Society Publication

Open Access

# Stimulated Brillouin Scattering Enhanced Fibers for Narrow-Band Filtering by Tailoring Brillouin Gain Spectrum

Volume 9, Number 6, December 2017

Zhen Guo
Changjian Ke
Chen Xing
Yibo Zhong
Guo Yin
Deming Liu

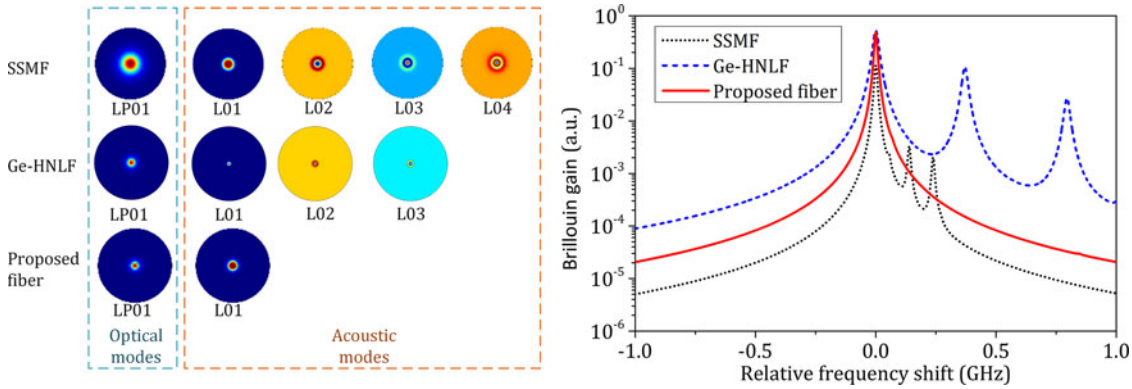


DOI: 10.1109/JPHOT.2017.2767679
1943-0655 © 2017 IEEE

# Stimulated Brillouin Scattering Enhanced Fibers for Narrow-Band Filtering by Tailoring Brillouin Gain Spectrum

**Zhen Guo**,[1] **Changjian Ke**,[1,2] **Chen Xing**,[1] **Yibo Zhong**,[1] **Guo Yin**,[1] **and Deming Liu**[1,2]

[1]School of Optical and Electronic Information, Huazhong University of Science and Technology, Wuhan 430074, China
[2]National Engineering Laboratory for Next Generation Internet Access System, Huazhong University of Science and Technology, Wuhan 430074, China

*DOI:10.1109/JPHOT.2017.2767679*


Manuscript received September 3, 2017; revised October 22, 2017; accepted October 24, 2017. Date of publication October 30, 2017; date of current version November 14, 2017. This work was supported by the National Natural Science Foundation of China (NSFC) under Grant 61475053. Corresponding author: C. Ke (e-mail: cjke@mail.hust.edu.cn).

**Abstract:** A novel highly nonlinear optical fiber with enhanced stimulated Brillouin scattering for narrow-band filtering is proposed. Herein, we initially discuss the tailoring of the Brillouin gain spectrum in germanium and fluorine co-doped single cladding fibers. By adjusting the fiber structure and the doping concentration, the excitation of optical and acoustic modes, as well as coupling efficiency between them, can be manipulated properly. Then a double cladding structure is introduced in order to mitigate the accompanying undesired four-wave mixing effect. The simulation results show that the Brillouin gain spectrum of the proposed fiber is composed of single peak, corresponding to the fundamental optical mode and fundamental acoustic mode. The Brillouin gain efficiency is $\sim$2.45 $m^{-1} \cdot W^{-1}$, and the bandwidth is $\sim$17 MHz. Finally, the experimental and simulated frequency responses of the narrow-band optical filter utilizing the proposed fiber are in good agreement.

**Index Terms:** Optical fibers, fiber nonlinear optics, optical filters.

## 1. Introduction

Stimulated Brillouin scattering (SBS) is one of the most prominent optical nonlinearities [1], which can be used in numerous applications, such as spectrum measurement [2]–[4], microwave photonics (MWP) [5], [6] and fiber-optic sensing [7], [8]. To some extent, the performance of SBS applications is related to the characteristics of the Brillouin gain spectrum (BGS). For example, there is a need for a BGS with multiple peaks to realize simultaneous distributed strain and temperature measurement [7], [9]. In contrast, a BGS with single peak is preferable for ultra-high resolution spectrometers and microwave photonic filters (MPF) since the gain response of the SBS process can be used as an optical filter [4]. Besides, high Brillouin gain coefficient can enhance the performance of these applications.

As is known, the SBS effect can be described classically as a nonlinear interaction between the pump and Stokes fields through an acoustic wave [1]. Once the threshold is reached, the backward-propagating Stokes wave carries most of the input power and the growth of it can be characterized by the BGS [1]. Actually, the characteristics of BGS are dominated by the optical modes and acoustic

modes guided in the core or the cladding [9]–[12]. By adjusting the waveguide structure and the doping concentration, the excitation of optical and acoustic modes, as well as coupling efficiency between them, can be manipulated properly. That is to say the BGS can be modified as desired. For example, a multi-peak BGS, which are contributed by the fundamental optical mode and multiple acoustic modes, can be observed in a w-shaped optical fiber with high-delta germanium-doped core and fluorine-doped inner cladding (F-HDF) [9] or a small core tellurite photonic crystal fiber (PCF) [12]. In addition, the fundamental optical and acoustic modes can be excited in a chalcogenide ($As_2S_3$) rib waveguide through SBS process, which results in a single-peak BGS [6], [13]. To the best of our knowledge, a fiber with a BGS featuring single passband, narrow bandwidth and high Brillouin gain coefficient for narrow-band filtering, has not been investigated yet.

For a better practical use of SBS-based filters, it's necessary to mitigate other nonlinear effects in fibers. For example, the accompanied four-wave mixing (FWM) can induce out-of-band gain in a reconfigurable SBS-based filter pumped by multiple lines, which can degrade the filter performance [14]. As is known, FWM process depends on the phase match and it's easy to satisfy the phase-matching condition near the zero-dispersion wavelength [1]. Hence, in order to minimize FWM, a specially designed fiber with dispersion tailoring is desired.

In this paper, a specially designed highly nonlinear fiber with a desired single-peak BGS is proposed. By adjusting the doping concentration as well as core radius of germanium and fluorine co-doped single-cladding fiber, the higher-order optical and acoustic modes are cut off and a relative large acousto-optic coupling coefficient between fundamental optical and acoustic modes can be achieved. Meanwhile, by introducing the double-cladding structure, the accompanying undesired FWM effect can be mitigated obviously. And the simulation results show that a highly nonlinear optical fiber with enhanced SBS effect, which has a 9.51-wt% germanium-doped, 1.75-$\mu$m radius core, a 2.79-wt% fluorine-doped, 2.28-$\mu$m inner cladding and a 2.29-wt% fluorine-doped outer cladding, is suitable for narrow-band filtering. It behaves a single-peak BGS with a bandwidth of $\sim$17 MHz and a Brillouin gain efficiency of $\sim$2.45 $m^{-1} \cdot W^{-1}$. Furthermore, the splice loss from the proposed novel fiber to the standard single mode fiber (SSMF) and the cutoff wavelength are also analyzed. Finally, the measured frequency response of the narrow-band optical filter based on the proposed fiber shows good agreement with the simulation result. And this proposed fiber has been used in high resolution spectrum measurement [15] and microwave photonics filtering [16].

## 2. Theoretical Analysis

It is well known that the characteristics of BGS are strongly related to the interaction between the optical and acoustic modes [10]. The field distributions of the optical modes $E$ and acoustic modes $u_m$ are determined by the optical eigenvalue (1) and the mechanical (2) [8]–[10]:

$$\nabla^2 \mathrm{E} + \left(\frac{2\pi}{\lambda}\right)^2 \left(\mathrm{n}^2 - \mathrm{n}_{\mathrm{eff}}^2\right) \mathrm{E} = 0 \tag{1}$$

$$\nabla^2 \mathrm{u}_m + \left(\frac{\Omega_m^2}{\mathrm{V}_l^2} - \beta_{ac}^2\right) \mathrm{u}_m = 0 \tag{2}$$

where $\lambda$ is the pump wavelength, $n$ is the refractive index, $n_{eff}$ is the effective refractive index, $V_l$ is the acoustic velocity, $f_{B,m} = \Omega_m / 2\pi$ is the Brillouin frequency shift contributed by the $m$-order acoustic mode, and $\beta_{ac}$ is the propagation constant of acoustic field. Here, we assume that the refractive index $n$ at a wavelength of 1550 nm and the acoustic velocity $V_l$ [m/s] would vary with the germanium concentration $wt_1$ [wt%] and fluorine concentration $wt_2$ [wt%] as [8]–[10]:

$$n = 1.458\left(1 + 1.0 \times 10^{-3} wt_1 - 3.3 \times 10^{-3} wt_2\right) \tag{3}$$

$$V_l = 5944\left(1 - 7.2 \times 10^{-3} wt_1 - 2.7 \times 10^{-2} wt_2\right) \tag{4}$$

Meanwhile, the normalized optical frequency $V_{op}$ and acoustic frequency $V_{ac}$ can be expressed as:

$$V_{op} = k_{op} a \sqrt{n_1^2 - n_2^2} \tag{5}$$

$$V_{ac} = \beta_{ac} a \sqrt{\left(\frac{V_{l0}}{V_{l1}}\right)^2 - \left(\frac{V_{l0}}{V_{l2}}\right)^2} \tag{6}$$

where $V_{l0}$ is the acoustic velocity of pure silica, $n_1$ and $n_2$ are the refractive indices in the core and cladding, and $V_{l1}$ and $V_{l2}$ are the acoustic velocities in the core and cladding, respectively. As is known, a step-index fiber supports a single optical mode if $V_{op} < 2.405$, and optical fibers designed to satisfy this condition are called single-mode fibers [1]. Similarly, single-acoustic-mode fibers support single acoustic mode if $V_{ac} < 3.8$ [8]. Furthermore, the process of the SBS effect is generated only when the phase-match condition is fulfilled [11]:

$$\beta_{ac} = 2\beta_{op} \tag{7}$$

where $\beta_{op} = 2\pi n_{eff}/\lambda$ is the propagation constant of the optical mode. In this condition, the guided optical and acoustic modes in fiber can be deduced by solving the two-dimensional scalar-wave equations of the optical eigenvalue (1) and the mechanical (2).

As we know, the BGS has a Lorentzian line shape and each acoustic mode contribution adds up in an incoherent way [10], [11]. Thus, the BGS can be computed by adding Lorentzian curves centered at each mode Brillouin frequency shift (BFS), which is given by [1], [10], [11]:

$$g_B(f) = \sum_m g_{B,m}^{Peak} \frac{(\Gamma_B/2)^2}{(f - f_{B,m})^2 + (\Gamma_B/2)^2} \tag{8}$$

where $1/\Gamma_B$ is the photon lifetime (typically $<$10 ns) [1], and $g_{B,m}^{Peak}$ is the peak Brillouin gain coefficient at $f = f_{B,m}$ and given by:

$$g_{B,m}^{Peak} = \frac{g_p \cdot I_m^{ac}}{A_{eff}} \tag{9}$$

in which $g_p \approx 5 \times 10^{-11}$ m/W is the intrinsic Brillouin gain coefficient, $I_m^{ac} \propto \int E^2 u_m$ is the acousto-optic coupling coefficient, which can be evaluated from the spatial overlap between optical mode $E$ and m-order acoustic mode $u_m$ field distributions, and $A_{eff}$ is the optical effective mode area.

## 3. Results and Discussion

Based on the theoretical analysis mentioned above, the optical and acoustic fields can be obtained by solving the optical eigenvalue (1) and the mechanical (2) respectively utilizing two-dimensional finite-element method (2D-FEM). Then the acousto-optic coupling coefficient $I_m^{ac}$ can be calculated, and the BGS can be easily deduced.

### 3.1 BGS Tailoring in Germanium-Doped Fibers

Firstly, we investigate the SBS process in germanium-doped fibers by changing the core radius $a$ and the acoustic velocity difference $\Delta V_l$ between the core and the cladding. Fig. 1 shows the excitation of optical and acoustic modes under different core radii $a$ and acoustic velocity differences $\Delta V_l$ in germanium-doped fibers. The influence of doping concentrations on acoustic velocity $V_l$ is given in (4). The refractive index difference $\Delta n$ is related to $\Delta V_l$ by the equation:

$$\Delta n = \frac{1.458}{5944 \times 7.2} \Delta V_l \tag{10}$$

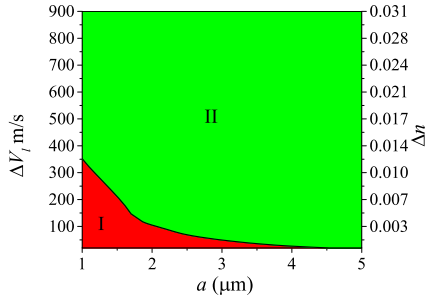


Fig. 1. Excitation of optical and acoustic modes under different core radii $a$ and acoustic velocity differences $\Delta V_l$ in germanium-doped fibers. I: single acoustic mode and single optical mode; II: multiple acoustic modes and single optical mode.

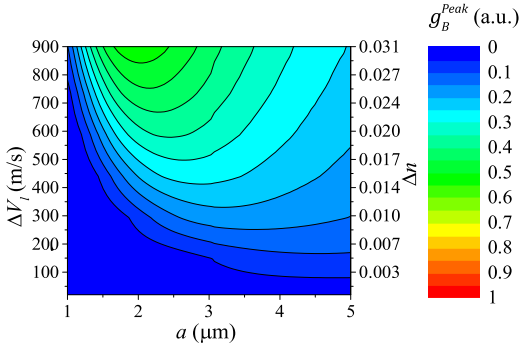


Fig. 2. Peak Brillouin gain coefficients $g_B^{Peak}$ as functions of different core radii $a$ and acoustic velocity differences $\Delta V_l$ in germanium-doped fibers.

In Fig. 1, it is obvious that higher-order acoustic modes tend to be excited with the increase of $a$ and $\Delta V_l$ as the normalized acoustic frequency $V_{ac}$ is larger than 3.8. For example, the BGS in SSMF is composed of multiple peaks, corresponding to multiple acoustic modes, as the $a$ and $\Delta V_l$ are about 4 $\mu$m and 120 m/s, respectively [11].

Furthermore, Fig. 2 shows the peak Brillouin gain coefficients $g_B^{peak}$ at the same parameters as those of Fig. 1. It can be observed that $g_B^{peak}$ increases when $\Delta V_l$ increases. This result can be understood by noting that the refractive index difference $\Delta n$ corresponding to $\Delta V_l$ increases according to (10). However, the maximum position corresponds to multiple acoustic modes in Fig. 1, which means a multi-peak BGS. For example, a Ge-HNLF has a relative high Brillouin gain coefficient but a multi-peak BGS [17]. From our discussion thus far, we expect that $\Delta n$ can increase while keeping $\Delta V_l$ reduced, ensuring that the optical modes can be confined tightly to the core without exciting the higher-order acoustic modes. In this condition, the BGS in fibers is composed of single peak with a relative high Brillouin gain coefficient. It is possible to get the higher-order acoustic modes suppressed as well as peak Brillouin gain coefficient increased by introducing a fiber composed of a germanium-doped core and a fluorine-doped cladding.

### *3.2 BGS Tailoring in Germanium and Fluorine Co-Doped Single Cladding Fibers*

As mentioned above, the refractive index $n$ and the acoustic velocity $V_l$ would vary with the different germanium and fluorine concentrations, as shown in (3) and (4). Particularly, Fig. 3 plots the doping concentration dependence of refractive index difference $\Delta n$ and acoustic velocity difference $\Delta V_l$ in a fiber with a germanium-doped core and a fluorine-doped cladding. It is worth noting that $\Delta n$ can be increased flexibly while $\Delta V_l$ keeps unchanged with appropriate dopant concentrations, which means it can provide independent control of the optical and acoustic modes.

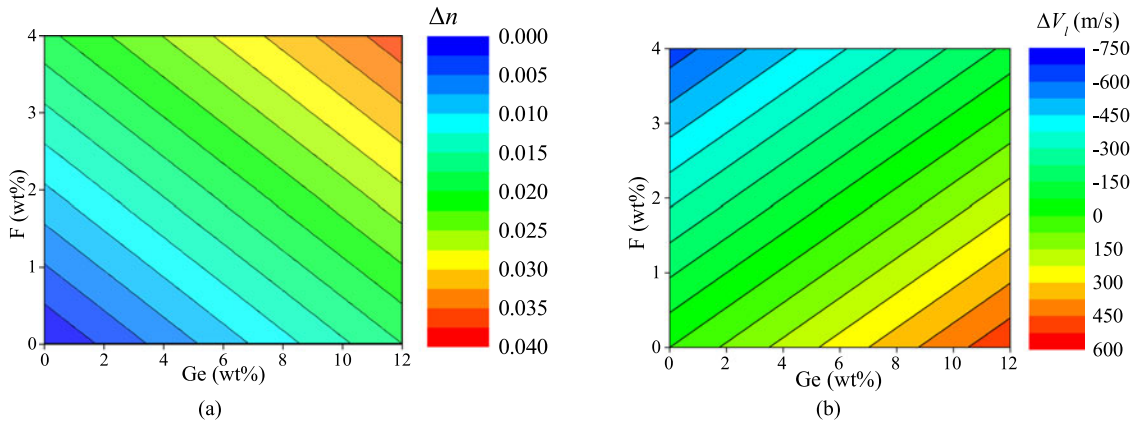


Fig. 3. Doping concentration dependence of refractive index difference $\Delta n$ and acoustic velocity difference $\Delta V_l$. Germanium and fluorine are doped in core and cladding, respectively.

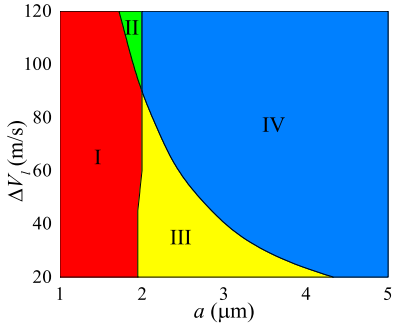


Fig. 4. Excitation of optical and acoustic modes under different core radii $a$ and acoustic velocity differences $\Delta V_l$ in germanium and fluorine co-doped single cladding fibers when refractive index difference $\Delta n = 0.03$. I: single acoustic mode and single optical mode; II: multiple acoustic modes and single optical mode; III: single acoustic mode and multiple optical modes; IV: multiple acoustic modes and multiple optical modes.

Fig. 4 illustrates the excitation of optical and acoustic modes under different core radii $a$ and acoustic velocity differences $\Delta V_l$ in germanium and fluorine co-doped single cladding fibers when refractive index difference $\Delta n = 0.03$. Similarly to Fig. 1, higher-order acoustic modes tend to be excited as $a$ and $\Delta V_l$ increase. At the same time, higher-order optical modes are excited in a large-core fiber with high $\Delta n$. Moreover, peak Brillouin gain coefficients $g_B^{peak}$ as functions of core radii $a$ and acoustic velocity differences $\Delta V_l$ when relative index difference $\Delta n = 0.03$ are plotted in Fig. 5. As can be seen in Fig. 5, it appears that the $g_B^{peak}$ increases with the decrease of $a$ from 5 $\mu$m to 2 $\mu$m because of the tight confinement of the optical and acoustic modes, and the maximum value occurs for a specific value of $a \approx 1.75\,\mu$m. When the core radius $a$ is reduced such that $a < 1.5\,\mu$m, the optical modes spread farther into the cladding, resulting a smaller values of $g_B^{peak}$. Besides, Fig. 6 denotes peak Brillouin gain coefficients $g_B^{peak}$ and bandwidths $B_w$ as functions of index differences $\Delta n$ in germanium and fluorine co-doped single cladding fibers with $a = 1.75\,\mu$m when acoustic velocity difference $\Delta V_l$ varies. It is obviously seen that $g_B^{peak}$ increases as $\Delta n$ increases. This implies that we ought to increase refractive index difference in order to enhance the peak Brillouin gain coefficient. However, Fig. 6 indicates that the bandwidth $B_w$ will degrade with the increasing of $\Delta n$. Thus, a compromise must be made between peak Brillouin gain coefficient and bandwidth.

We also investigate the dispersion parameters $D_C$ of germanium and fluorine co-doped single cladding fibers with the same core radius $a = 1.75\,\mu$m and $\Delta n = 0.03$ but different acoustic velocity difference $\Delta V_l$, as shown in Fig. 7. A small dispersion parameter ($\sim -3.3$ ps/nm/km at $\lambda =$

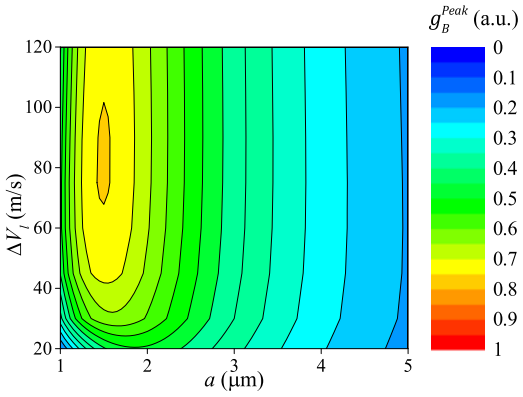


Fig. 5. Peak Brillouin gain coefficients $g_B^{Peak}$ as functions of core radii a and acoustic velocity differences $\Delta V_l$ in germanium and fluorine co-doped single cladding fibers when relative index difference $\Delta n = 0.03$.

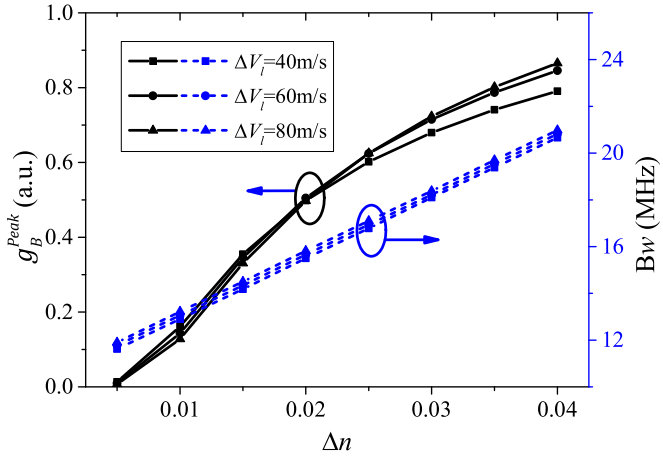


Fig. 6. Peak Brillouin gain coefficients $g_B^{Peak}$ and bandwidths $B_w$ as functions of index differences $\Delta n$ in germanium and fluorine co-doped single cladding fibers with a = 1.75 $\mu$m when acoustic velocity difference $\Delta V_l$ varies.

1550 nm) is observed for each fiber. In this condition, FWM occurs very easily and will degrade the performance of SBS applications. For example, in order to obtain a filter with rectangular gain spectrum using Lorentzian-shape SBS gain, a pump consisting of equal-amplitude spectral lines is required. The flat optical frequency comb actually leads to uneven SBS gain due to the influence of FWM, as shown in Fig. 8. Thus, in order to mitigate the incalculable gain induced by FWM effect among the multiple pump lines, an SBS enhanced fiber with an improved $D_C$ is strongly desired.

### 3.3 BGS Tailoring in Germanium and Fluorine Co-Doped Double Cladding Fibers

To avoid the influence of FWM, we introduce the double cladding structure as shown in Fig. 9. The double cladding structure with a fluorine-doped depressed inner cladding is employed to precisely control the dispersive properties of the fiber.

Fig. 10 shows the excitation of optical and acoustic modes under different inner and outer fluorine concentration differences $\Delta$F and ratios between inner cladding radius and core radius Ra in germanium and fluorine co-doped double cladding fibers when acoustic velocity difference $\Delta V_l$ varies. It is seen that higher-order acoustic modes tend to be excited as $\Delta$F and Ra increase because fluorine-doped inner cladding acts as an enhanced waveguide layer for acoustic modes.

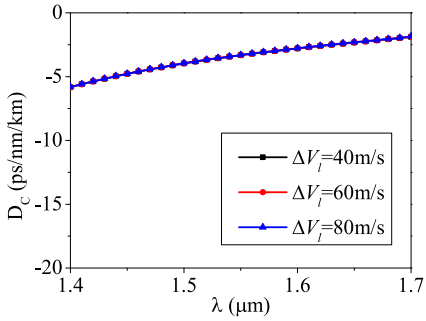


Fig. 7. Dispersion parameters $D_C$ of germanium and fluorine co-doped single cladding fibers with $a = 1.75\ \mu$m and $\Delta n = 0.03$ under different acoustic velocity difference $\Delta V_l$.

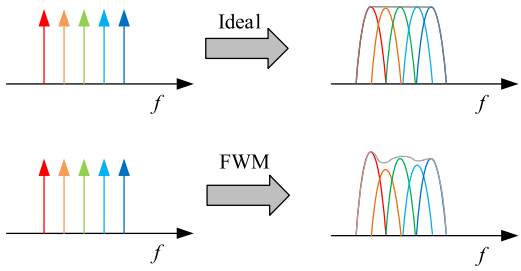


Fig. 8. Influence of FWM on the SBS-based filter passband flatness.

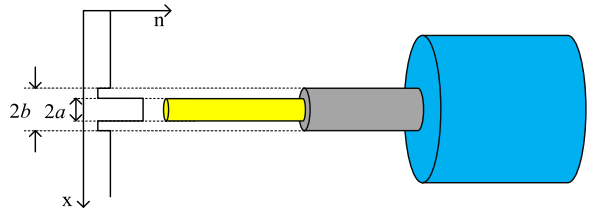


Fig. 9. Structures of germanium and fluorine co-doped double cladding fibers

Similarly, Fig. 11 illustrates peak Brillouin gain coefficients at the same parameters as those of Fig. 10. It can be clearly seen that the peak Brillouin gain coefficient decreases as the ΔF and Ra increase.

In addition, Fig. 12 shows the dispersion parameters $D_C$ and dispersion slopes $S_D$ at the wavelength of 1550 nm as functions of ΔF and Ra in double cladding fibers when $\Delta V_l = 40$ m/s. The results indicate that the absolute value of $D_C$ increases as ΔF increases and an improvement of $D_C$ can be observed with an appropriate Ra. Hence, the relative larger absolute value of $D_C$ can lead to an adequate phase mismatch between adjacent wavelength channels so that FWM in the germanium and fluorine co-doped double cladding fiber can be suppressed effectively. What's more, the dispersion slope $S_D$ varies from $-0.002$ ps/nm/km to 0.018 ps/nm/km, which means the double cladding fiber has adequate chromatic dispersion coefficient over wide wavelength region.

According to the previous discussion, Table 1 summarizes the characteristics of the proposed fiber. It is worth noting that the Brillouin gain efficiency of the proposed fiber is enhanced compared with that of the SSMF, and an adequate chromatic dispersion can be obtained in order to mitigate FWM. Additionally, the splice loss from the proposed fiber to SSMF is about 2.02 dB due to the poor mode match between them. Moreover, low-loss splices can be achieved by some novel methods, such as repeated arc discharges [18] and fusion splicers [19]. What's more, for all the fibers considered, the cutoff wavelength $\lambda_{cc}$ can meet the requirements of C- and L-band applications.

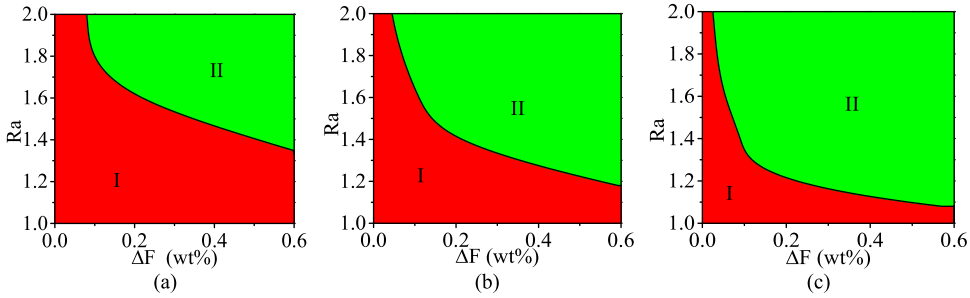


Fig. 10. Excitation of optical and acoustic modes under inner and outer fluorine concentration differences ΔF and ratios between inner cladding radius and core radius Ra in germanium and fluorine co-doped double cladding fibers when acoustic velocity difference $\Delta V_l$ varies. I: single acoustic mode and single optical mode; II: multiple acoustic modes and single optical mode. (a) $\Delta V_l = 40$ m/s. (b) $\Delta V_l = 60$ m/s. (c) $\Delta V_l = 80$ m/s.

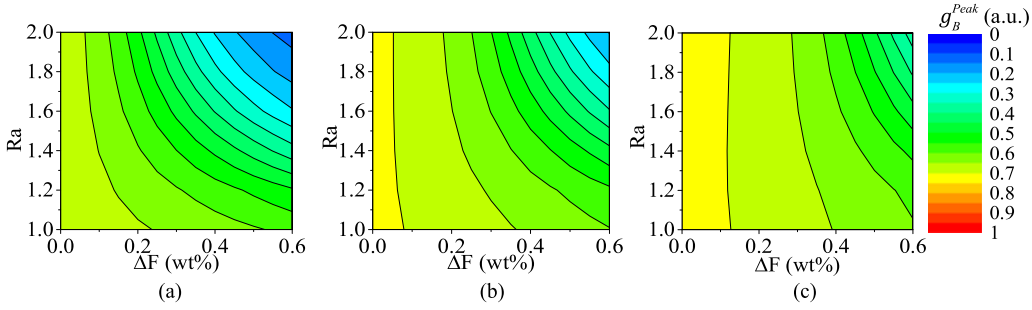


Fig. 11. Peak Brillouin gain coefficients $g_B^{Peak}$ as functions of inner and outer fluorine concentration differences ΔF and ratios between inner cladding radius and core radius Ra in germanium and fluorine co-doped double cladding fibers when acoustic velocity difference $\Delta V_l$ varies. (a) $\Delta V_l = 40$ m/s. (b) $\Delta V_l = 60$ m/s. (c) $\Delta V_l = 80$ m/s.

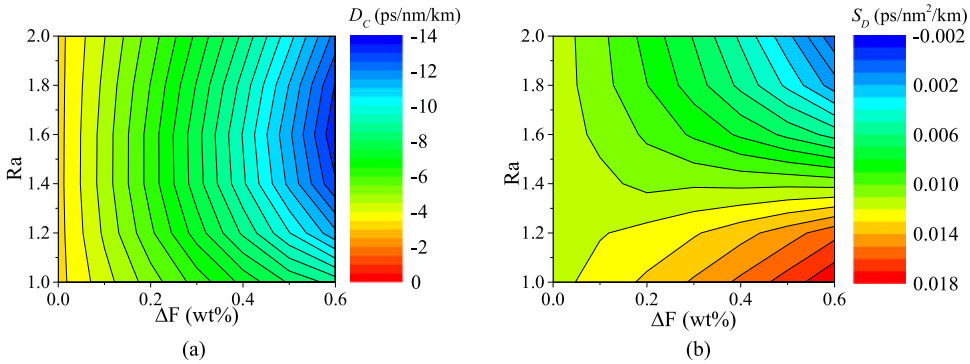


Fig. 12. Dispersion parameters $D_C$ (a) and dispersion slopes $S_D$ (b) as functions of inner and outer fluorine concentration differences ΔF and ratios between inner cladding radius and core radius Ra in germanium and fluorine co-doped double cladding fibers when acoustic velocity difference $\Delta V_l =$ 40 m/s.

Fig. 13(a) plots the field distributions of optical and acoustic modes in SSMF, Ge-HNLF and the proposed fiber. All of them support single optical mode, but the SSMF and Ge-HNLF have multiple acoustic modes while our proposed fiber supports single acoustic mode. Furthermore, Fig. 13(b) illustrates the simulated BGS in SSMF, Ge-HNLF and the proposed fiber. The SSMF and Ge-HNLF both have a germanium-doped core and a pure silica cladding. We can find that the BGS in SSMF and Ge-HNLF is mainly composed of multiple peaks, which is in good agreement

Table 1
Characteristics of the Proposed Fiber

| Characteristics | Conditions | Specified Values | Units |
|---|---|---|---|
| Effective mode area | 1550 nm | 15.568 | $\mu m^2$ |
| Nonlinear index coefficient | | $2.9650 \times 10^{-20}$ | $m^2/W$ |
| Nonlinear coefficient | 1550 nm | 7.7 | $(W \cdot km)^{-1}$ |
| Peak Brillouin gain efficiency | | 2.4529 | $(W \cdot m)^{-1}$ |
| SBS threshold × effective length | 1550 nm | 8.5613 | W·m |
| Brillouin gain bandwidth | | 17 | MHz |
| Dispersion parameter | 1550 nm | −10.673 | ps/nm/km |
| Dispersion slope | 1550 nm | 0.0128 | $ps/nm^2/km$ |
| Splice loss to SSMF | 1550 nm | 2.0226 | dB |
| Cutoff wavelength | | <1400 | nm |
| Numerical aperture | | 0.2696 | |

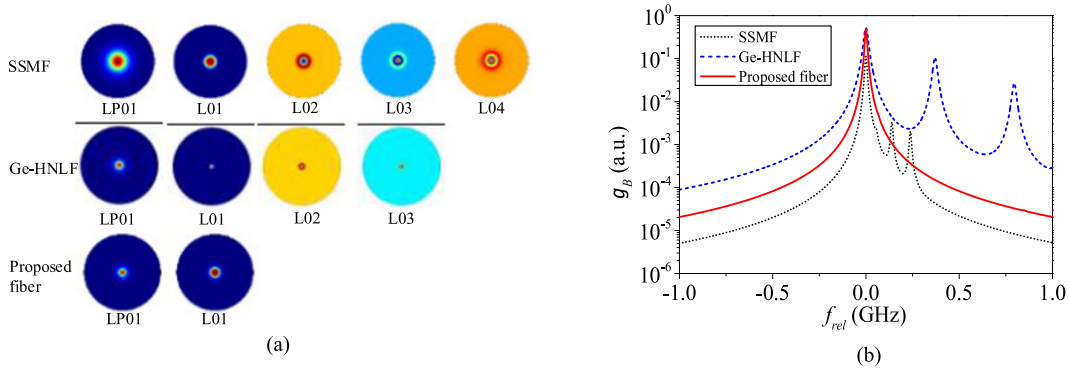


Fig. 13. Cross section of optical and acoustic modes (a) and Simulated BGS (b) in SSMF, Ge-HNLF and the proposed fiber. $g_B$: Brillouin gain coefficients, $f_{rel}$: relative frequency shift.

with the results reported in [12] and [17]. The proposed fiber has a germanium-doped core, a fluorine-doped depressed inner cladding and a fluorine-doped outer cladding. The core radius is 1.75 $\mu$m and the germanium concentration is 9.51 wt%. The inner cladding radius is 2.28 $\mu$m, and the fluorine concentrations of the inner cladding and the outer cladding are 2.79 wt% and 2.29 wt% respectively. The results show that the BGS in the proposed fiber is composed of single peak and the peak Brillouin gain is much higher than that of SSMF. Meanwhile, the bandwidth of BGS in the proposed fiber is ∼17 MHz.

Furthermore, Fig. 14 illustrates the simulated amplitude and phase response of SBS-based narrow-band filter utilizing the proposed fiber. The fiber length is 2 km, the signal power is −60 dBm, and the pump power is 9 dBm. It can be seen from Fig. 14 that an optical filter with a selectivity of ∼50 dB can be achieved and the linear correlation coefficient $R^2$ of the phase response is about 0.9998. Similarly, the experimental amplitude response is shown in Fig. 15. The fiber length is 2 km, the signal power is −60 dBm, and the pump power is 13 dBm. Pump power in experiment is higher than that in simulation owing to losses in experiment setup. Fig. 15 indicates that the measured frequency response is consistent with the simulated result. The experimental result has been reported previously by our team in [20]. Additionally, this kind of proposed fiber has been

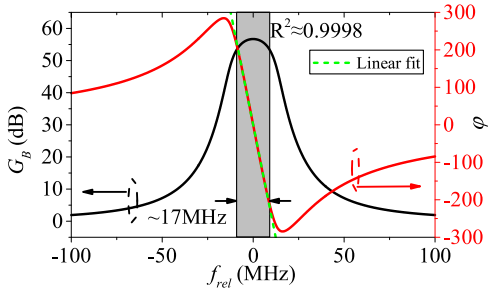


Fig. 14. Simulated amplitude and phase response of SBS-based filter utilizing the proposed fiber. $G_B$: Brillouin gain, $\varphi$: relative phase, $f_{rel}$: relative frequency shift.

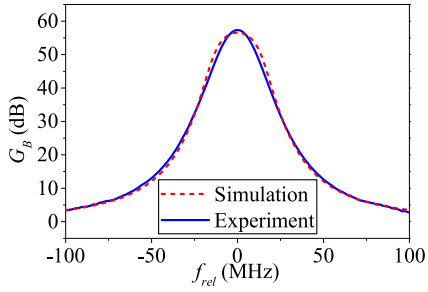


Fig. 15. Experimental and simulated results of frequency response of SBS-based filter utilizing the proposed fiber [20]. $G_B$: Brillouin gain, $f_{rel}$: relative frequency shift.

employed in high resolution spectrum measurement [15] and microwave photonics [16]. The fiber length is reduced from 20 km to 2 km without degrading the performance of the SBS applications. The resolution of the high-resolution spectroscopy is ~10 MHz and the selectivity of microwave photonic filter is >49 dB.

## 4. Conclusion

We propose a novel highly nonlinear fiber with enhanced SBS effect for narrow-band optical filter. By optimizing the doping level as well as structure of germanium and fluorine co-doped single cladding fiber, the BGS can be tailored precisely as desired and a high Brillouin gain coefficient can be obtained. Meanwhile, by introducing the double cladding structure, the accompanying undesired FWM effect can be mitigated to some degree. The results show that a desired BGS with singe peak and bandwidth of ~17 MHz can be achieved. The peak Brillouin gain efficiency is ~2.45 $m^{-1} \cdot W^{-1}$, much higher than that of SSMF. Additionally, the splice loss from proposed fiber to SSMF is discussed and the cutoff wavelength of proposed fiber can meet the demand of C- and L-band applications. Furthermore, the experimental and simulated frequency responses of the narrow-band optical filter utilizing the proposed fiber are in good agreement. This proposed fiber has been used in spectrum measurement and microwave photonics filtering and high performance can be achieved.

## References

[1] G. P. Agrawal, *Nonlinear Fiber Optics*. Singapore: Elsevier, 2007.
[2] Y. Dong *et al.*, "Sub-MHz ultrahigh-resolution optical spectrometry based on Brillouin dynamic gratings," *Opt. Lett.*, vol. 39, no. 10, pp. 2967–2970, May 2014.
[3] K. Zhang, C. Ke, D. Pan, and D. Liu, "High resolution optical spectrum measurement utilizing a dual-stage SBS-based filter," in *Proc. Asia Commun. Photon. Conf. 2015*, Nov. 2015, Paper AS4C.6.

[4] W. Wei, L. Yi, Y. Jaouën, and W. Hu, "Software-defined microwave photonic filter with high reconfigurable resolution," *Sci. Rep.*, vol. 6, Oct. 2016, Art. no. 35621.
[5] J. Ge and M. P. Fok, "Ultra high-speed radio frequency switch based on photonics," *Sci. Rep.*, vol. 5, Oct. 2015, Art. no. 17263.
[6] R. Pant, D. Marpaung, I. V. Kabakova, B. Morrison, C. G. Poulton, and B. J. Eggleton, "On-chip stimulated Brillouin scattering for microwave signal processing and generation," *Laser Photon. Rev.*, vol. 8, no. 5, pp. 653–666, Sep. 2014.
[7] M. A. Soto, G. Bolognini, F. Di Pasquale, and L. Thévenaz, "Simplex-coded BOTDA fiber sensor with 1 m spatial resolution over a 50 km range," *Opt. Lett.*, vol. 35, no. 2, pp. 259–261, Jan. 2010.
[8] F. Gao *et al.*, "On-chip high sensitivity laser frequency sensing with Brillouin mutually-modulated cross-gain modulation," *Opt. Express*, vol. 21, no. 7, pp. 8605–8613, Apr. 2013.
[9] W. Zou, Z. He, and K. Hotate, "Acoustic modal analysis and control in w-shaped triple-layer optical fibers with highly-germanium-doped core and F-doped inner cladding," *Opt. Express*, vol. 16, no. 14, pp. 10006–10017, Jan. 2008.
[10] Y. Koyamada, S. Sato, S. Nakamura, H. Sotobayashi, and W. Chujo, "Simulating and designing Brillouin gain spectrum in single mode fibers," *J. Lightw. Technol.*, vol. 22, no. 2, pp. 631–639, Feb. 2004.
[11] Y. Sikali Mamdem *et al.*, "Two-dimensional FEM analysis of Brillouin gain Spectra in acoustic guiding and antiguiding single mode optical fibers," in *Proc. COMSOL Multiphys. Conf. (Session Acoustic II, Paris, 2010)*, 2010, pp. 111–124.
[12] R. Cherif, A. B. Salem, T. S. Saini, A. Kumar, R. K. Sinha, and M. Zghal, "Design of small core tellurite photonic crystal fiber for slow-light-based application using stimulated Brillouin scattering," *Opt. Eng.*, vol. 54, no. 7, Jul. 2015, Art. no. 075101.
[13] B. J. Eggleton, B. Luther-Davies, and K. Richardson, "Chalcogenide photonics," *Nature Photon.*, vol. 5, no. 3, pp. 141–148, Feb. 2011.
[14] W. Wei, L. Yi, Y. Jaouen, M. Morvan, and W. Hu, "Brillouin rectangular optical filter with improved selectivity and noise performance," *IEEE Photon. Technol. Lett.*, vol. 27, no. 15, pp. 1593–1596, Aug. 2015.
[15] C. Xing, C. Ke, K. Zhang, Z. Guo, Y. Zhong, and D. Liu, "Polarization- and wavelength-independent SBS-based filters for high resolution optical spectrum measurement," *Opt. Express*, vol. 25, no. 7, pp. 20969–20982, Sep. 2017.
[16] K. Zhang, Y. Zhong, C. Ke, and D. Liu, "High-input dynamic range and selectivity stimulated Brillouin scattering-based microwave photonic filter utilizing a dual-stage scheme," *Opt. Lett.*, vol. 42, no. 17, pp. 3287–3290, Sep. 2017.
[17] M. Hirano, T. Nakanishi, T. Okuno, and M. Onishi, "Silica-based highly nonlinear fibers and their application," *IEEE J. Sel. Topics Quantum Electron.*, vol. 15, no. 1, pp. 103–113, Feb. 2009.
[18] L. Xiao, W. Jin, and M. S. Demokan, "Fusion splicing small-core photonic crystal fibers and single-mode fibers by repeated arc discharges," *Opt. Lett.*, vol. 32, no. 2, pp. 115–117, Dec. 2006.
[19] O. Fraz˜ao, J. P. Carvalho, and H. M. Salgado, "Low-loss splice in a microstructured fibre using a conventional fusion splicer," *Microw. Opt. Tech. Let.*, vol. 46, no. 2, pp. 172–174, Jan. 2005.
[20] K. Zhang, C. Ke, D. Pan, and D. Liu, "High resolution and selectivity SBS-based filter utilizing a dual-stage scheme," in *Proc. Opt. Fiber Commun. Conf.*, Mar. 2016, Paper W3E.5.